Intrasubband plasmons in semi-infinite *n-i-p-i* semiconductor superlattices

Manvir S. Kushwaha
Instituto de Física, Universidad Autónoma de Puebla, Apartado Postal J-48, Puebla-72570, Mexico
(Received 5 September 1991)

A theoretical investigation has been made of the collective intrasubband plasma modes in a semi-infinite superlattice system consisting of *n*- and *p*-type doped semiconductors separated by an undoped intrinsic (*i*) semiconductor (*n-i-p-i* superstructure). The thicknesses of the constituent layers are assumed to be sufficiently large so that quantum-well effects can be ignored. The material layers are characterized by frequency-dependent (macroscopic) dielectric functions. The nonradiative plasma modes are defined by the electromagnetic fields that decay exponentially away from each interface and that have an envelope that decays exponentially away from the end of the truncated superlattice. We employ a fully retarded theory in the framework of a transfer-matrix method. The general dispersion relations are shown to reproduce exactly the theoretical results for a binary semiconductor (or dielectric) superlattice. Numerical examples are presented for several illustrative cases.

I. INTRODUCTION

Modern crystal-growth techniques, such as molecular-beam epitaxy and metal-organic chemical-vapor deposition, have made possible the synthesis of crystalline semiconductor heterostructures with a specified band gap. Because of their applications as potentially useful devices, the physics of these artificial semiconducting heterostructures and superlattices has attracted a great deal of interest in the past decade.[1] It has been shown that such tailor-made superstructures possess electronic and optical properties, not seen in the host semiconductors, arising from the predetermined quantum states of two-dimensional character.[2] The knowledge of elementary collective excitations in the superlattice systems is of fundamental importance to the understanding of the electronic and optical properties. The collective excitations include phonons, magnons, plasmons, and polaritons, which have been studied both theoretically and experimentally.

The collective (bulk and surface) plasmon-polaritons in binary compositional semiconducting superlattices have been studied extensively in the recent past. These studies have been carried out both in the absence[3–8] and in the presence[9–14] of an external magnetic field. The lowering of symmetry caused by an applied magnetic field has been shown to produce interesting qualitative changes in the behavior characteristic of the plasmon-polaritons (for instance, the nonreciprocal propagation in the Voigt geometry[11] and a large Zeeman-like splitting in the perpendicular geometry.[12–14]).

In contrast to compositional superlattices, the *n-i-p-i* semiconducting superlattices, which were also included in original proposal,[1] have received relatively less attention theoretically as well as experimentally. A greater part of work on the electronic and optical properties of *n-i-p-i* superlattices has been pursued by Döhler and Ploog.[15] The effect of an external magnetic field on the plasmons in the finite *n-i-p-i* superlattice in the Voigt geometry was considered by Johnson and Camley.[16] The propagation of bulk and surface plasmon-polaritons in the *n-i-p-i* structure with charge carriers strictly confined to the interfaces was considered by Farias, Auto, and Albuquerque.[17] Recently, this work has been extended by subjecting the finite *n-i-p-i* structure to an external magnetic field in the Voigt geometry.[18]

The aim of the present work is to investigate the collective (bulk and surface) excitations in the *n-i-p-i* semiconducting superlattices in the "classical limit." The term "classical limit" is used here to refer to the situation in which the layer thicknesses are large enough so that the quantum-well effects can be neglected and the constituent layers can be described by macroscopic dielectric functions. We develop a fully retarded theory in the framework of a transfer-matrix method to obtain the general dispersion relations. The existence of the surface plasmon-polaritons has been successfully substantiated. It is found that the highest polariton mode does not behave properly in the long-wavelength limit if $d_B/d_A > 1$, where d_A and d_B are, respectively, the layer thicknesses of the surface layer and the first intrinsic layer.

The rest of the paper is organized as follows. In Sec. II we review the transfer-matrix formalism used to obtain the general dispersion relations for the bulk and surface collective excitations. In Sec. III we present numerical examples for several illustrative cases. We consider the asymptotic limits attained by the bulk plasmon bands and the surface plasmon-polaritons in Sec. IV. Finally, Sec. V is devoted to summarizing our theoretical results.

II. FORMALISM

The superlattice structure considered in the present paper is depicted in Fig. 1. Material layers *A*, *B*, *C*, and *D* have frequency-dependent dielectric functions ϵ_A, ϵ_B, ϵ_C, and ϵ_D and layer thicknesses d_A, d_B, d_C, and d_D, respectively. The period of the superlattice structure is defined

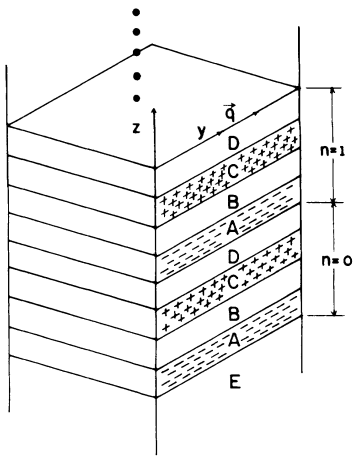

FIG. 1. Schematics of the superlattice geometry considered in this paper. Material layers A, B, C, and D are, respectively, n-doped, intrinsic, p-doped, and intrinsic semiconductors, with respective thicknesses d_i, $i \equiv A,B,C,D$. The integer n refers to the number of unit cell. The semi-infinite medium E ($-\infty \leq z < 0$) is an insulator.

as $d = d_A + d_B + d_C + d_D$. The plasma modes are assumed to propagate along the y direction parallel to the interfaces with wave vector q_y and frequency ω. We are interested in the collective excitations characterized by the electromagnetic (EM) fields localized at and decaying exponentially away from the interfaces. Although the whole formalism is quite general where the unit cell of the superlattice is assumed to be composed of four different material layers (all characterized by frequency-dependent dielectric functions), we will later specify our analytic results corresponding to the *n-i-p-i* superlattice.

A. Infinite superlattice

We start with the general wave-field equation in terms of the macroscopic electric field ($\mathbf{E}$) in the absence of an applied magnetic field:

$$\nabla \times (\nabla \times \mathbf{E}) - q_0^2 \epsilon \mathbf{E} = \mathbf{0} , \tag{1}$$

where $q_0 = \omega/c$ is the vacuum wave vector. We assume the spatial and temporal dependence of the EM fields to be of the form $\sim e^{i(\mathbf{q}\cdot\mathbf{r}-\omega t)}$. In Eq. (1) $\epsilon \equiv \epsilon(\omega)$ is the scalar dielectric function for the medium in which the wave equation is being applied. In the present situation, Eq. (1) can be written as

$$\begin{bmatrix} q_0^2\epsilon - q_y^2 - q_z^2 & 0 & 0 \\ 0 & q_0^2\epsilon - q_z^2 & q_y q_z \\ 0 & q_y q_z & q_0^2\epsilon - q_y^2 \end{bmatrix} \begin{bmatrix} E_x \\ E_y \\ E_z \end{bmatrix} = \begin{bmatrix} 0 \\ 0 \\ 0 \end{bmatrix} . \tag{2}$$

In writing Eq. (2) we have used the fact that in the situation at hand the dielectric function $\epsilon(\omega)$ is simplified by the symmetry requirements such that $\epsilon_{xx} = \epsilon_{yy} = \epsilon_{zz} = \epsilon$ and $\epsilon_{xy} = \epsilon_{yx} = \epsilon_{yz} = \epsilon_{zy} = \epsilon_{xz} = \epsilon_{zx} = 0$. The dielectric function relevant to the present situation is defined as

$$\epsilon(\omega) = \epsilon_L \left[1 - \frac{\omega_p^2}{\omega^2} \right] , \tag{3}$$

where ϵ_L is the background dielectric constant and ω_p is the plasma frequency of the medium concerned. The system of Eqs. (2) admits a nontrivial solution only if the determinant of the coefficient matrix vanishes. This leaves us with the following result:

$$-q_z^2 = \alpha^2 = q_y^2 - q_0^2 \epsilon(\omega) . \tag{4}$$

We write the field solutions in the four media (of the unit cell) as follows:

$$\mathbf{E}(\mathbf{r},t) = \mathbf{E}(z) e^{i(q_y y - \omega t)} , \tag{5}$$

where $\mathbf{E}(z)$ for each layer of the nth cell is given by

$$\mathbf{E}_j^{(n)}(z) = \mathbf{E}_{1j}^{(n)} e^{\alpha_j z} + \mathbf{E}_{2j}^{(n)} e^{-\alpha_j z} , \tag{6}$$

where $j \equiv A,B,C,D$. Analogous field solutions can be written for the magnetic field variable $\mathbf{B}$ in the respective layers.

The standard EM boundary conditions are the continuity of the tangential electric- and magnetic-field components: E_x, E_y, B_x, and B_y. Note that, in the absence of an applied magnetic field, only two boundary conditions at each interface are sufficient; we therefore decide to match E_y and B_x field components at the interfaces. In order to simplify the calculation, we reduce the number of unknown amplitudes by expressing B_x in terms of E_y. For the sake of brevity, we henceforth suppress the script y in $E_{ylj}^{(n)}$, with $l \equiv 1,2$ and $j \equiv A,B,C,D$, and choose to replace $E_{lj}^{(n)}$ by $j_l^{(n)}$, with $j \equiv A,B,C,D$. As such, we write the boundary conditions so that

$$\underline{M}_A |A_l^{(n)}\rangle = \underline{N}_B |B_l^{(n)}\rangle \quad \text{at } z = nd + d_A , \tag{7}$$

$$\underline{M}_B |B_l^{(n)}\rangle = \underline{N}_C |C_l^{(n)}\rangle \quad \text{at } z = nd + d_A + d_B , \tag{8}$$

$$\underline{M}_C |C_l^{(n)}\rangle = \underline{N}_D |D_l^{(n)}\rangle \quad \text{at } z = nd + d_A + d_B + d_C , \tag{9}$$

$$\underline{M}_D |D_l^{(n)}\rangle = \underline{N}_A |A_l^{(n+1)}\rangle \quad \text{at } z = (n+1)d , \tag{10}$$

where $|j_l^{(n)}\rangle$, with $j \equiv A,B,C,D$ and $l \equiv 1,2$, are column vectors and $\underline{M}_j$ and $\underline{N}_j$ are 2×2 matrices defined by

$$\underline{M}_j = \begin{bmatrix} e^j & e^{-j} \\ n_j e^j & -n_j e^{-j} \end{bmatrix}, \quad \underline{N}_j = \begin{bmatrix} 1 & -1 \\ n_j & -n_j \end{bmatrix} , \tag{11}$$

where

$$n_j = \epsilon_j/\alpha_j, \quad e^j = e^{\alpha_j d_j}; \quad j \equiv A,B,C,D . \tag{12}$$

From Eqs. (7)–(10), it is easy to see that

$$|A_l^{(n+1)}\rangle = \underline{T} |A_l^{(n)}\rangle , \tag{13}$$

where $\underline{T}$ is a 2×2 matrix defined by

$$\underline{T} = \underline{N}_A^{-1} \underline{M}_D \underline{N}_D^{-1} \underline{M}_C \underline{N}_C^{-1} \underline{M}_B \underline{N}_B^{-1} \underline{M}_A . \tag{14}$$

The matrix $\underline{T}$ in this equation is a transfer matrix which relates the coefficients of EM fields in the two consecutive cells. In order to account for the periodicity of the superlattice system, we impose Bloch's ansatz defined by

$$|A_l^{(n+1)}\rangle = e^{iQ}|A_l^{(n)}\rangle \ , \tag{15}$$

where $Q=kd$, with $k\equiv q_z$, is a dimensionless Bloch wave vector. Substituting Eq. (15) in Eq. (13) yields

$$[\underline{T}-e^{iQ}\underline{I}]|A_l^{(n)}\rangle = 0 \ , \tag{16}$$

where $\underline{I}$ is a 2×2 unit matrix. Since $|A_l^{(n)}\rangle$ is an arbitrary (general) vector of the superlattice system at hand, the nontrivial solutions are given by the condition

$$|\underline{T}-e^{iQ}\underline{I}| = 0 \ . \tag{17}$$

The explicit form of the $\underline{T}$ matrix is relegated to the Appendix. Using the fact that $\det(\underline{T})=1$, Eq. (17) can be shown to assume the form

$$\cos Q - \tfrac{1}{2}\,\mathrm{tr}\underline{T} = 0 \ . \tag{18}$$

This is the simplified general dispersion relation for the collective (bulk) excitations of the four-layer superlattice system under consideration. We have examined Eq. (18) by subjecting it to the special limits, viz, $d_B=d_D=0$. It can readily be seen that Eq. (18), for this limit, reproduces exactly the dispersion relation for the collective (bulk) excitations in a binary semiconducting superlattice [see Eq. (23) in Ref. 8].

B. Truncated superlattice

In order to study the surface plasmon-polaritons in the superlattice system we consider the geometry when the superstructure is truncated at $z=0$ such that the medium E in the region $-\infty \le z \le 0$ is replaced by an insulator with a dielectric constant ϵ_E. We seek solutions to Maxwell's equations in which the EM fields are localized at each interface of the superlattice as well as at the interface between the insulator and the first layer of the superlattice. Note that the matching of the boundary conditions at $z=0$ is equivalent to those at $z=nd$ with $n=0$. The result is

$$A_1^{(0)} + A_2^{(0)} = E_y^{(E)} \ , \tag{19}$$

$$n_A A_1^{(0)} - n_A A_2^{(0)} = n_E E_y^{(E)} \ , \tag{20}$$

where

$$n_E = \epsilon_E/\alpha_E, \quad \alpha_E^2 = q_y^2 - q_0^2\epsilon_E \ . \tag{21}$$

Eliminating $E_y^{(E)}$ from Eqs. (19) and (20) gives

$$\beta A_1^{(0)} - A_2^{(0)} = 0 \ , \tag{22}$$

where

$$\beta = (n_A - n_E)/(n_A + n_E) \ . \tag{23}$$

Since the polariton modes are characterized by the exponentially decaying fields, we use the ansatz in Eq. (15) by replacing Q by $i\lambda$ and write Eq. (17) for the vector $|A_l^{(0)}\rangle$. The result is

$$(T_{11}-e^{-\lambda})A_1^{(0)} + T_{12}A_2^{(0)} = 0 \ , \tag{24}$$

$$T_{21}A_1^{(0)} + (T_{22}-e^{-\lambda})A_2^{(0)} = 0 \ . \tag{25}$$

The condition that Eqs. (22) and (24) have a nontrivial solution can be written in the form

$$e^{-\lambda} = T_{11} + \beta T_{12} \ . \tag{26}$$

Similarly, the condition that Eqs. (22) and (25) have a nontrivial solution takes the form

$$e^{-\lambda} = T_{22} + \frac{1}{\beta}T_{21} \ . \tag{27}$$

The dispersion relation for the surface plasmon-polaritons in the truncated superlattice system is obtained by equating the two expressions for $e^{-\lambda}$ given by Eqs. (26) and (27). The result is

$$\beta(T_{11}+\beta T_{12}) = T_{21} + \beta T_{22} \ . \tag{28}$$

Equation (28) has been checked by imposing special limits, viz., $d_B=d_D=0$. It is found that our general dispersion relation, within these limits, reproduces exactly the proper results for the collective (surface) excitations in a binary semiconducting superlattice [see Eq. (31) in Ref. 8].

It is noteworthy that the general formalism of the four-layer superlattice can easily be transformed corresponding to an *n-i-p-i* semiconducting superlattice. For this purpose, we assume that the constituent layers A and C are, respectively, n- and p-type doped and B and D are the intrinsic semiconductors. Consequently, the plasma frequency $\omega_{pA}\equiv\omega_{pe}$, $\omega_{pC}\equiv\omega_{ph}$, and $\omega_{pB}=0=\omega_{pD}$. Moreover, *n-i-p-i* superlattices can be fabricated with any single semiconductor as the host material, since there are no restrictions on the choice of materials due to the requirements of lattice matching. In view of this, we have made an extensive numerical computation for the *n-i-p-i* semiconductor superlattice made up of a single host material.

III. NUMERICAL EXAMPLES

In this section we present numerical examples for the dispersion relations. The analytical results derived in the preceding section describe collective excitations which can arise from many different microscopic mechanisms. We plot our numerical results in terms of the dimensionless frequency $\xi=\omega/\omega_{pe}$, dimensionless wave vector $\zeta=cq_y/\omega_{pe}$, and the dimensionless layer thicknesses $\delta_A=\omega_{pe}d_A/c$, $\delta_B=\omega_{pe}d_B/c$, $\delta_C=\omega_{pe}d_C/c$, and $\delta_D=\omega_{pe}d_D/c$. Since the existence of plasmon-polaritons depends upon the relative magnitude of the layer thicknesses, we have presented several illustrative cases.

The material parameters used in the present computation are ϵ_L $(=\epsilon_{LA}=\epsilon_{LB}=\epsilon_{LC}=\epsilon_{LD})=13.13$; $\epsilon_E=1.0$; $n_h=n_e$, $m_h^*=2m_e^* \Longrightarrow \omega_{ph}=\omega_{pe}/\sqrt{2}$; $\delta_A \ge \delta_B,\delta_C,\delta_D;\delta_A \le \delta_B,\delta_C,\delta_D$. Here n_i and m_i^* are, respectively, the carrier concentration and the effective mass $i\equiv e,h$. The plasma frequency of the intrinsic layers $\omega_{pB}=0=\omega_{pD}$. The subscripts e and h refer to electrons (layer A) and holes (layer C), respectively.

A. $\delta_A \geq \delta_B, \delta_C, \delta_D$

The first case that we consider is illustrated by the specific example $\delta_A = 1.0$, $\delta_B = 0.5$, $\delta_C = 1.0$, $\delta_D = 0.5$. The results are shown in Fig. 2. There are four bulk plasmon bands (BPB) shown by the shaded regions and four surface plasmon-polaritons (SPP) plotted as the dotted curves. The lower pair of BPB starts from the origin, observes a gap between the two with the increasing ζ, and approaches the same asymptotic limit at large ζ. The upper pair of BPB starts from the light line ($\alpha_E = 0$) with a gap between the two, except at the value of reduced wave vector $\zeta \simeq 2.0$. The upper pair of BPB also reaches the same asymptotic limit. The lowest SPP starts from the origin and propagates in the gap between the lower pair of BPB to merge into the upper edge of the lowest BPB at large ζ. The second-lowest SPP starts from the light line ($\alpha_E = 0$) in the gap between the two pairs of BPB, changes its group velocity twice during the course of propagation, and finally merges into the upper BPB of the lower pair of BPB. The third-lowest SPP starts from the light line ($\alpha_E = 0$) within the gap between the upper pair of BPB, propagates with exactly the same characteristics as the second-lowest SPP, and never merges into either of the BPB. The uppermost SPP starts from the upper edge of the uppermost BPB and approaches the asymptotic limit assigned by $\epsilon_A + \epsilon_E = 0$.

The other examples in this case are shown by reducing thickness of the *p*-doped medium (layer *C*) to $\delta_C = 0.75$ (Fig. 3) and $\delta_C = 0.5$ (Fig. 4). It is found that the gap between the lower pair of BPB increases with decreasing the thickness of the *p*-doped layer. Similarly, the gap between the upper pair of BPB increases at the small wave vectors and their touching point appears at relatively large wave vectors. Apart from a minor difference in the

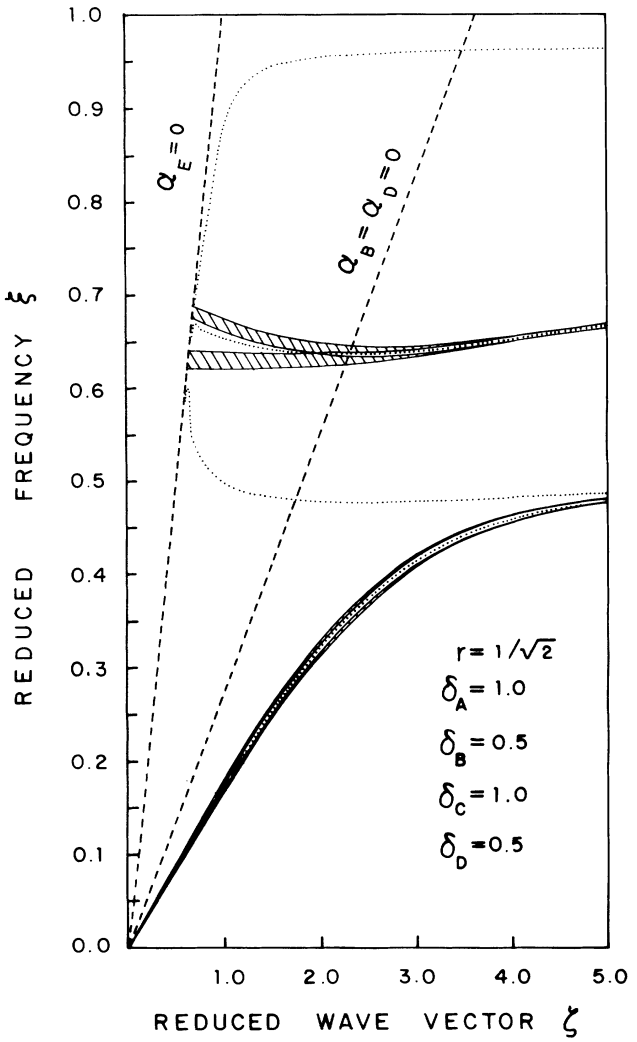

FIG. 2. Dispersion curves for the surface plasmon-polaritons (dotted curves) of the truncated superlattice and the allowed bulk bands (shaded regions) of the infinite superlattice. The symbol r is defined as $r = \omega_{ph}/\omega_{pe}$. The dashed lines marked $\alpha_E = 0$ and $\alpha_B = \alpha_D = 0$ are the light lines, respectively, in the media E and B (or D). The parameters used are listed in the figure.

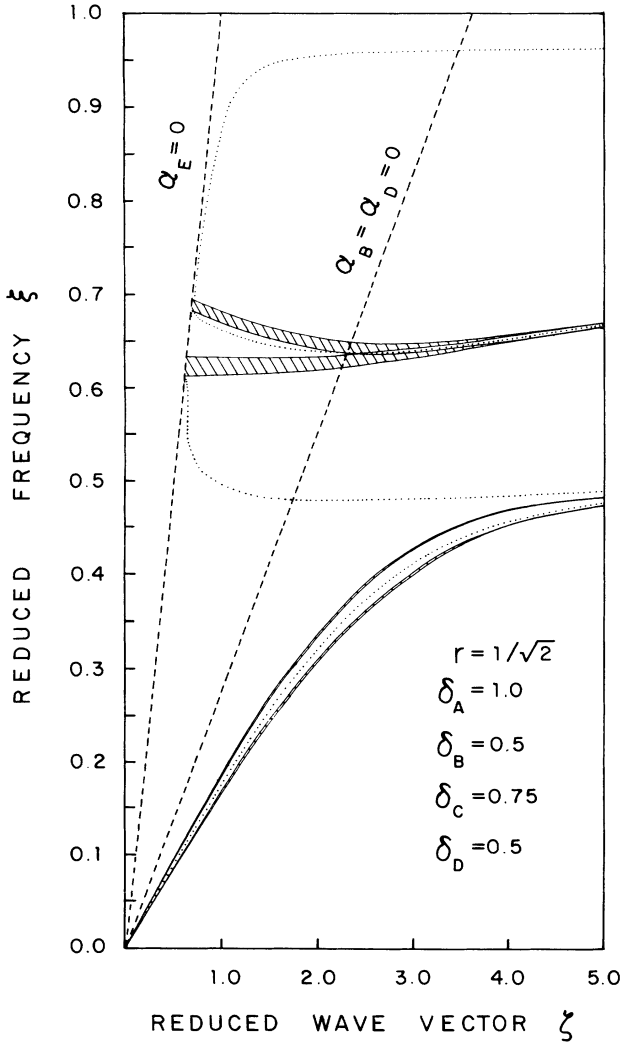

FIG. 3. Dispersion curves for the surface plasmon-polaritons (dotted curves) of the truncated superlattice and the allowed bulk bands (shaded regions) of the infinite superlattice. The parameters used are listed in the figure.

frequencies of the BPB and SPP, particularly at small wave vectors, the rest of the discussion regarding their propagation characteristics related to Fig. 2 is still valid.

The case of equal layer thicknesses with $\delta_A=\delta_B=\delta_C=\delta_D=1.0$ is depicted in Fig. 5. A significant difference occurs in the reduction of the spatial gap between the two pairs of the BPB due to an increase (decrease) in the frequencies of the lower (upper) BPB at small wave vectors. The frequencies of the lowest SPP increase and those of the second-lowest and the third-lowest SPP decrease, particularly at small wave vectors. As a result the uppermost SPP starts at relatively smaller frequencies. It is noteworthy that while the lowest SPP is a pure polariton mode over the whole wave vector range, the upper three SPP modes retain their pure polariton character only towards the right of light line marked $\alpha_B=\alpha_D=0$ where λ, α_A, α_B, α_C, α_D, and α_E are all real and positive.

B. $\delta_A \leq \delta_B, \delta_C, \delta_D$

The first case we consider here is demonstrated by the specifying $\delta_A=0.5$, $\delta_B=1.0$, $\delta_C=0.5$, and $\delta_D=1.0$. The numerical results are plotted in Fig. 6. There are several significant differences as compared to previous cases. The widths of all the BPB are found to increase when the thickness of the surface layer (A) is smaller or equal to that of the interior layers. The frequencies of the lowest SPP increase and those of the second-lowest and third-lowest SPP decrease as compared to the previous examples. A remarkable difference is seen in the propagation characteristic of the uppermost SPP mode which does not behave properly towards the left of the light line marked $\alpha_B=\alpha_D=0$, particularly at the small wave vectors where the retardation effect is stronger. We have devoted a separate figure (Fig. 10) to discuss the strange behavior of this mode.

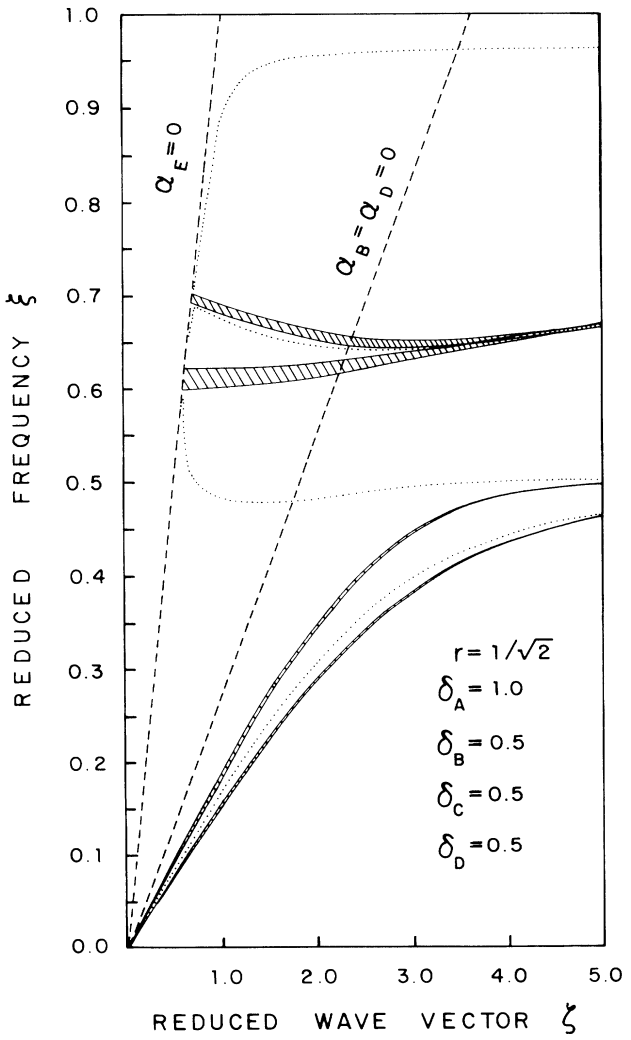

FIG. 4. Dispersion curves for the surface plasmon-polaritons (dotted curves) of the truncated superlattice and the allowed bulk bands (shaded regions) of the infinite superlattice. The parameters used are listed in the figure.

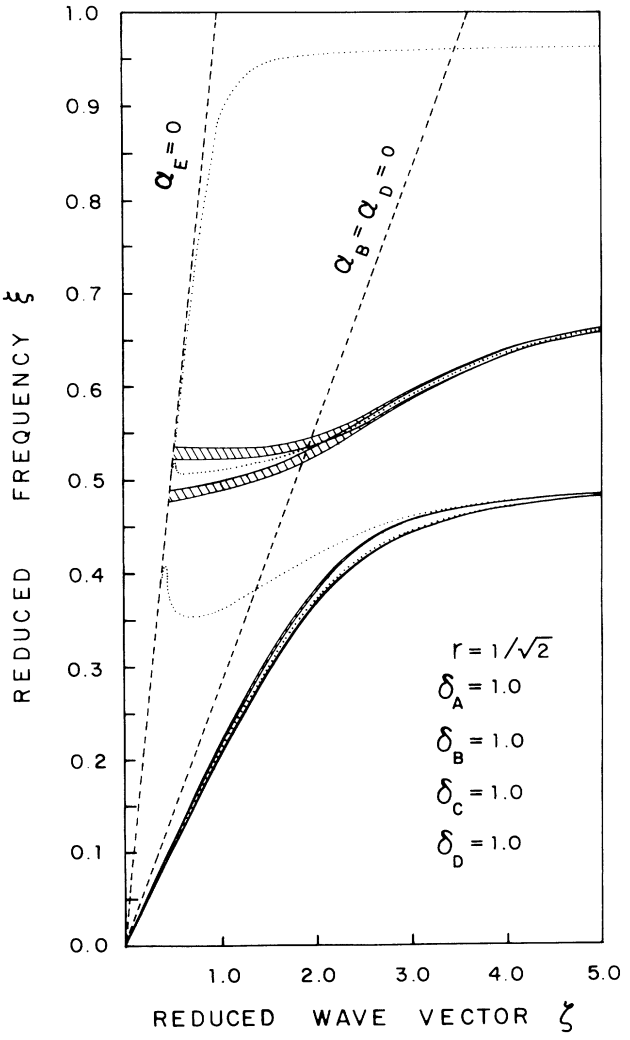

FIG. 5. Dispersion curves for the surface plasmon-polaritons (dotted curves) of the truncated superlattice and the allowed bulk bands (shaded regions) of the infinite superlattice. The parameters used are listed in the figure.

The case of increasing the thickness of the *p*-doped layer is illustrated by the examples $\delta_C = 0.75$ (Fig. 7) and $\delta_C = 1.0$ (Fig. 8). It is seen that the frequencies of the lowest and the second-lowest SPP modes increase, while those of the third-lowest SPP mode decrease at small wave vectors. The gap between the lower pair of the BPB reduces and the touching point between the upper pair of the BPB tends to move towards smaller wave vectors. In fact, the touching point between the upper pair of the BPB disappears altogether (Fig. 8).

The last example we consider in this case is shown, for the equal layer thicknesses with $\delta_A = \delta_B = \delta_C = \delta_D = 0.5$, in Fig. 9. However, it seems to be more pertinent to compare the results in Fig. 9 with those in Fig. 5 of the preceding subsection. Thus it is seen that the widths of the BPB increase with decreasing the layer thicknesses. The gap between the lower as well as the upper pair of BPB increases. The touching point of the upper pair of BPB moves towards the lower wave vector. The frequencies of the lowest SPP mode decrease whereas those of the second-lowest and third-lowest ones increase, with decreasing layer thicknesses, at the small wave vectors. The remark made about the uppermost SPP mode in Figs. 6–8 is, however, still valid.

Finally, we comment on the difference in the behavior characteristic of the uppermost SPP mode when $\delta_A < \delta_B \leq 1$. For this purpose, we have plotted this mode for several values of δ_A keeping δ_B, δ_C, and δ_D constant. It can be seen that when $\delta_A < \delta_B$, this SPP mode does not propagate the way it does when $\delta_A \geq \delta_B \leq 1$, and observes a kind of resonance splitting in the wave-vector range $(1 \lesssim \zeta \lesssim 2.5)$ where the retardation effect is important. The magnitude of the resonance splitting (measured in terms of the vertical distance) is found to increase with decreasing δ_A. We understand that the important factors which play simultaneously a significant role in restraining this mode to attain a pure polariton character in this situation and in this range of propagation are the following.

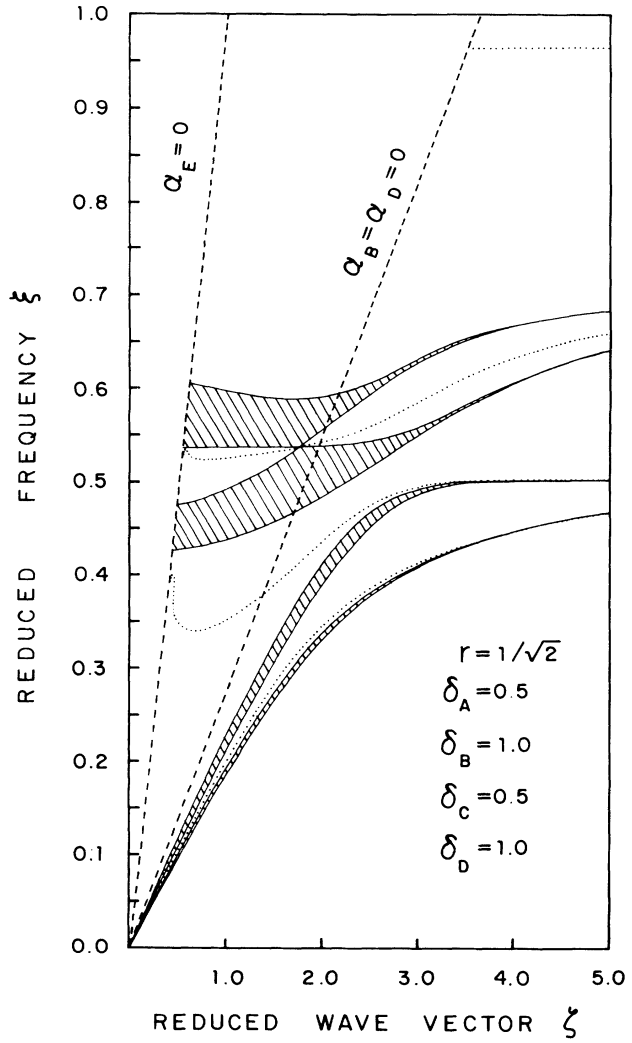

FIG. 6. Dispersion curves for the surface plasmon-polaritons (dotted curves) of the truncated superlattice and the allowed bulk bands (shaded regions) of the infinite superlattice. The parameters used are listed in the figure.

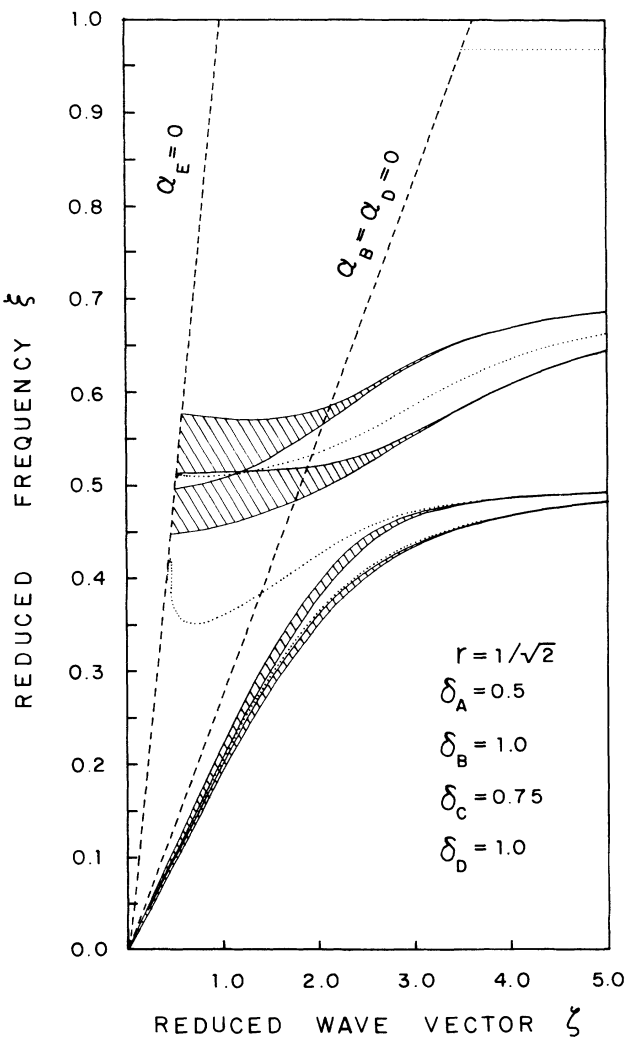

FIG. 7. Dispersion curves for the surface plasmon-polaritons (dotted curves) of the truncated superlattice and the allowed bulk bands (shaded regions) of the infinite superlattice. The parameters used are listed in the figure.

First, the decay constants α_B and α_D (and even α_C) are purely imaginary in this range. Remember, we do not mean that this is not so in other cases where the uppermost surface mode behaves properly. Second, when $\delta_A < \delta_B$, the semi-infinite medium ($-\infty \le z \le 0$) interacts presumably easily with the intrinsic layer B. This means that this surface mode is virtually describable by the relation

$$q_y^2 = q_0^2 \frac{\epsilon_E \epsilon_B}{\epsilon_E + \epsilon_B} ,$$

where ϵ_E ($=1.0$) and ϵ_B ($=\epsilon_L = 13.13$) are both positive quantities. This leads us to infer that the two "surface-wave-inactive" media in contact with each other will not support true polariton modes. The splitting of this mode, as seen at $\zeta \simeq 2.25$ in Fig. 10, is understood to take place due to the resonance interaction between the constituent layers.

IV. ANALYTICAL DIAGNOSIS—ASYMPTOTIC LIMITS

In the preceding section we demonstrated that the bulk plasmon bands in the infinite superlattice and the surface plasmon-polaritons in the semi-infinite superlattice become asymptotic to certain characteristic frequencies in the nonretarded limit ($c \to \infty$). In this section we focus on the analytical diagnosis of the exact dispersion relations in order to understand the asymptotic limits attained by the bulk bands and the surface modes.

Let us first recall the general dispersion relation for the collective (bulk) excitations, Eq. (18). In the nonretarded limit, this reduces to (see Appendix)

$$P_1 P_2 \equiv (n_A + n_D)(n_D + n_C)(n_C + n_B)(n_B + n_A)$$
$$\equiv (\epsilon_A + \epsilon_D)(\epsilon_D + \epsilon_C)(\epsilon_C + \epsilon_B)(\epsilon_B + \epsilon_A) = 0 , \quad (29)$$

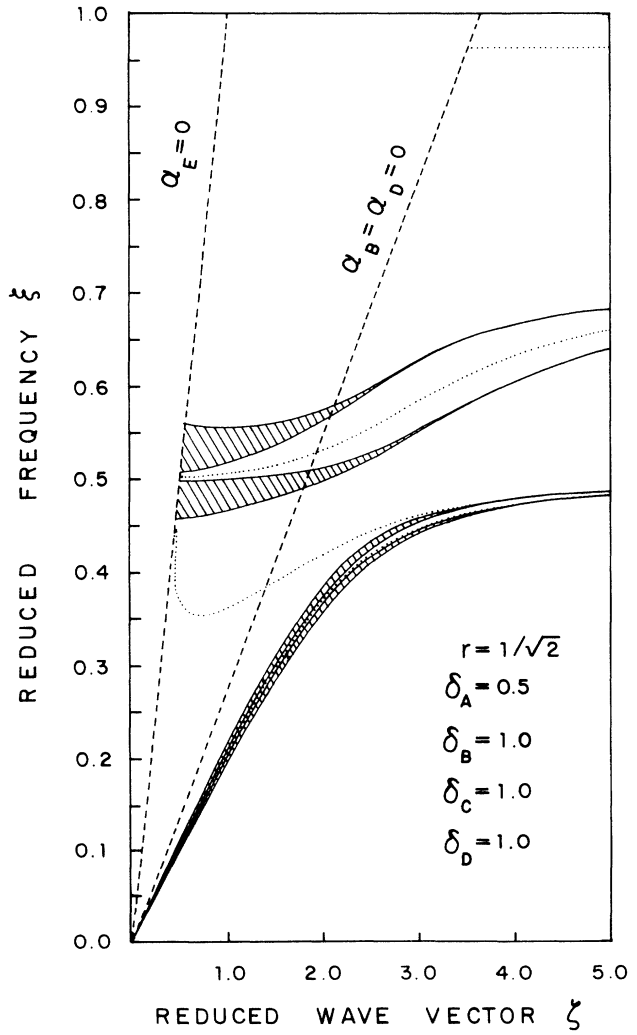

FIG. 8. Dispersion curves for the surface plasmon-polaritons (dotted curves) of the truncated superlattice and the allowed bulk bands (shaded regions) of the infinite superlattice. The parameters used are listed in the figures.

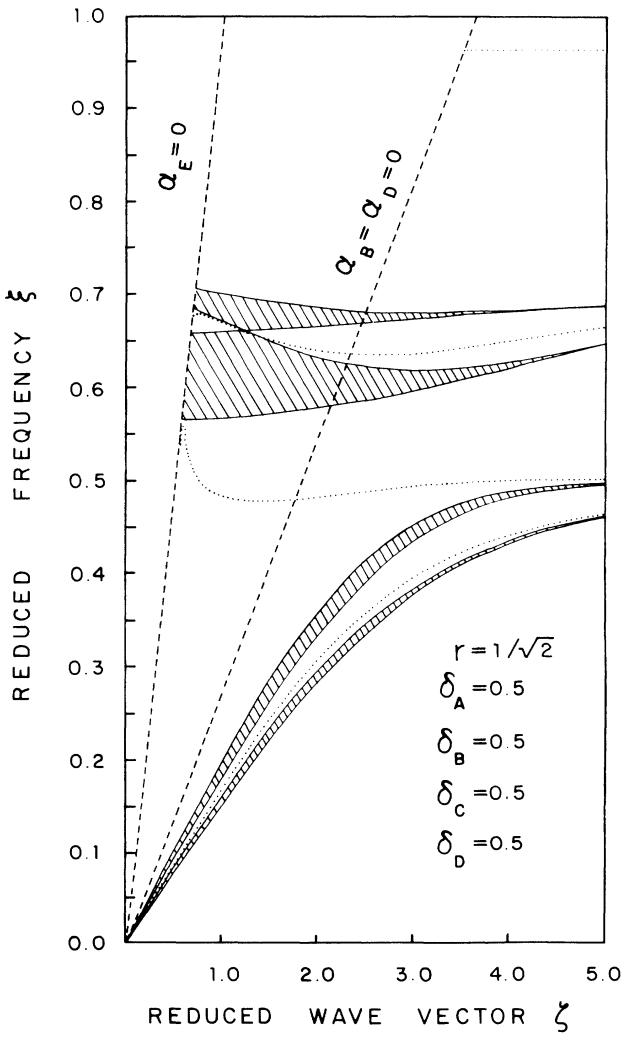

FIG. 9. Dispersion curves for the surface plasmon-polaritons (dotted curves) of the truncated superlattice and the allowed bulk bands (shaded regions) of the infinite superlattice. The parameters used are listed in the figure.

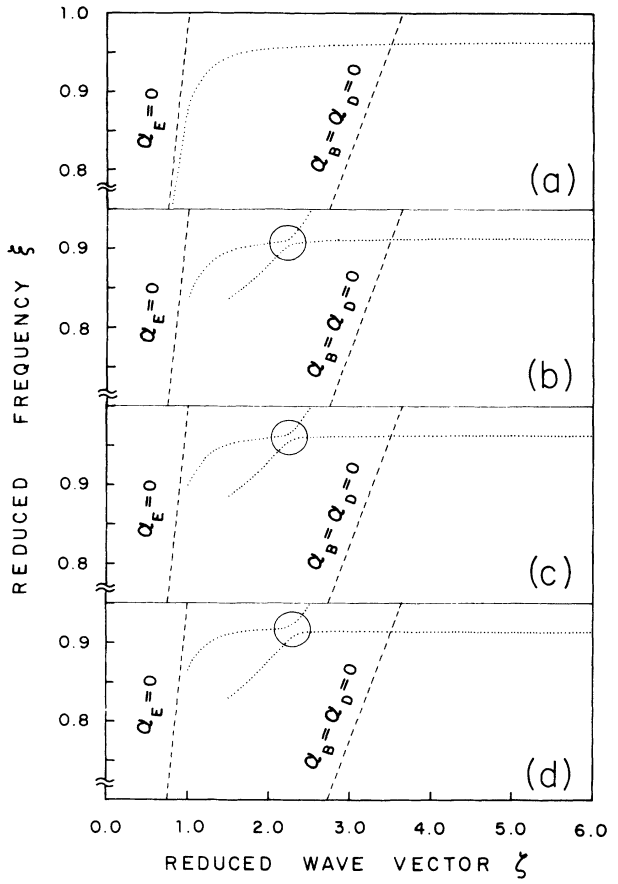

FIG. 10. Dispersion characteristic of the uppermost surface mode. (a) $\delta_A=\delta_B=\delta_C=\delta_D=1.0$; (b) $\delta_A=0.9$, $\delta_B=\delta_C=\delta_D=1.0$; (c) $\delta_A=0.7$, $\delta_B=\delta_C=\delta_D=1.0$; (d) $\delta_A=0.5$, $\delta_B=\delta_C=\delta_D=1.0$. We call attention to the resonance splitting (encircled regions) at the frequency specified by $\epsilon_A+\epsilon_E=0$ [see Eq. (37)].

where

$$\left.\begin{aligned}
&\epsilon_A=\epsilon_L\left[1-\frac{\omega_{pe}^2}{\omega^2}\right] \text{ for } n\text{-doped layer } A\ ,\\
&\epsilon_B=\epsilon_L \text{ for intrinsic layer } B\ ,\\
&\epsilon_C=\epsilon_L\left[1-\frac{\omega_{ph}^2}{\omega^2}\right] \text{ for } p\text{-doped layer } C\ ,\\
&\epsilon_D=\epsilon_L \text{ for intrinsic layer } D\ .
\end{aligned}\right\} \tag{30}$$

Since $\epsilon_B=\epsilon_D$, the third equality in Eq. (29) yields two possible solutions:

$$\epsilon_B+\epsilon_A=0 \tag{31}$$

or

$$\epsilon_C+\epsilon_B=0\ . \tag{32}$$

Equation (31), with the aid of Eqs. (30), yields

$$\xi=\frac{\omega}{\omega_{pe}}=\frac{1}{\sqrt{2}}\ , \tag{33}$$

and Eq. (32) gives

$$\xi=\frac{\omega}{\omega_{pe}}=\frac{1}{\sqrt{2}}\frac{\omega_{ph}}{\omega_{pe}}\ . \tag{34}$$

Equations (33) and (34), for the parameters used in the present numerical examples, reproduce exactly the frequencies approached, respectively, by the upper and the lower pairs of the bulk bands in the nonretarded limits (see, e.g., Figs. 2–9).

Similarly, Eq. (28), which is the dispersion relation for the collective (surface) excitations, in the nonretarded limit assumes the form (see Appendix)

$$\beta_2 P_2(\beta_1 P_1-\beta_2 R_1)=0\ , \tag{35}$$

where

$$\beta_1=n_A-n_E,\quad \beta_2=n_A+n_E\ , \tag{36}$$

and the rest of the symbols are as defined in the Appendix. Equating the first prefactor in Eq. (35) to zero gives

$$\beta_2\equiv(n_A+n_E)\equiv(\epsilon_A+\epsilon_E)=0$$

or

$$\xi=\frac{\omega}{\omega_{pe}}=\left[1+\frac{\epsilon_E}{\epsilon_L}\right]^{-1/2}\ . \tag{37}$$

The second prefactor, in Eq. (35), equated to zero yields

$$P_2\equiv(n_C+n_B)(n_B+n_A)\equiv(\epsilon_C+\epsilon_B)(\epsilon_B+\epsilon_A)=0\ . \tag{38}$$

The last equality in this equation reproduces exactly the two solutions given by Eqs. (31) and (32) and hence by Eqs. (33) and (34).

The third factor in Eq. (35) equated to zero gives

$$\begin{aligned}
(\beta_1 P_1-\beta_2 R_1)&\equiv(n_D+n_C)[(n_A-n_E)(n_A+n_D)-(n_A+n_E)(n_A-n_D)]\\
&\equiv(\epsilon_D+\epsilon_C)[(\epsilon_A-\epsilon_E)(\epsilon_A+\epsilon_D)-(\epsilon_A+\epsilon_E)(\epsilon_A-\epsilon_D)]\\
&=0\ .
\end{aligned} \tag{39}$$

Setting the first factor in the last equality to zero yields $\epsilon_D+\epsilon_C=\epsilon_D+\epsilon_B=0$, which is exactly the same as Eq. (32) and hence Eq. (34).

The second factor in the last equality in Eq. (39) equated to zero can be written as

$$2\epsilon_A(\epsilon_D-\epsilon_E)=0 \ . \tag{40}$$

Now $\epsilon_A\neq 0$, otherwise Eq. (31) can never be satisfied. Similarly, $\epsilon_D-\epsilon_E$ does not vanish since $\epsilon_D\neq\epsilon_E$. Thus the second factor in the last equality in Eq. (39) does not vanish.

In conclusion, it is established that the uppermost polariton mode approaches the asymptotic limit specified by Eq. (37). The third-lowest polariton mode reaches the same asymptotic limit as the upper pair of the bulk plasmon bands which is defined by Eq. (33). The lowest and the second-lowest polariton modes approach the asymptotic limit specified by Eq. (34), which is also the asymptotic limit attained by the lower pair of the bulk plasmon bands.

V. CONCLUSION

The purpose of this paper has been to investigate the dispersion characteristics of the collective (bulk and surface) excitations in an *n-i-p-i* semiconducting superlattice. The model theory presented in the framework of a transfer-matrix method has the advantage of being simpler and describes the analytical results in a compact form which are otherwise quite involved. While we have confined our attention to the case of a superlattice comprised of a single semiconductor as the host material, the theory quite clearly applies to the superlattice system made up of different host materials. Considering the moderate thicknesses of the constituent layers justifies the use of macroscopic dielectric functions and the neglect of quantum-well effects. The approximate analytical diagnosis presented in Sec. IV has proved to be very useful in understanding the asymptotic limits attained by the bulk plasmon bands and the surface plasmon polaritons in the short-wavelength limit. The analytical derivations are independent of any particular model. For instance, one can easily incorporate the effect of free-carrier collisions and of the coupling to the optical phonons.

The numerical examples presented in this paper exhibit various significant features. Let us first comment on the situation provided by the bulk bands. It is seen that there are four bulk plasmon bands—two of which start from the origin and approach the same asymptotic limit as described by Eq. (34) and the other two start from the light line ($\alpha_E=0$) with a gap between the two, except at a reduced wave vector where their inner edges touch each other. The latter pair of bulk bands attains the asymptotic limit specified by Eq. (33). It is found that the magnitude of the gap, both between the lower and upper pairs of the bulk bands, is inversely proportional to the width of the *p*-doped layer. The same is true about the occurrence of the touching point of the inner edges of the upper pair of the bulk bands.

There are four surface plasmon-polariton modes in the frequency interval $0\leq\xi\leq 1$. The lowest one starts from at the origin, propagates within the gap between the lower pair of the bulk bands, and merges into the upper edge of the lowest bulk band in the short-wavelength limit. The second-lowest mode starts from at the light line ($\alpha_E=0$) in the gap between the lower and the upper pairs of bulk bands, and changes the sign of its group velocity twice before merging into the upper edge of the second-lowest bulk band. The third-lowest polariton mode also starts from at the light line ($\alpha_E=0$) and propagates within the gap between the upper pair of the bulk bands without merging into either of these two bands until finally it, together with the two bands, approaches the asymptotic limit. The uppermost polariton mode, which attains exactly the same asymptotic limit as the one approached by the surface or interface polariton propagating at an interface $z=0$, has a varied story regarding its behavior in the wave-vector range where the retardation effect is important. It is found that in the situation that $\delta_A>\delta_B$ this mode behaves properly (see Figs. 2–5), whereas in the case that $\delta_A<\delta_B$ its polariton character is perturbed and it observes a resonance splitting due, possibly, to the interaction between the constituent layers. This is shown by some specific examples in Fig. 10 relevant to Figs. 6–9.

Attractive possibilities for the experimental observation of the surface plasmon-polariton modes predicted in the truncated *n-i-p-i* semiconductor superlattices are the attenuated total reflection or Raman (or, inelastic light) scattering techniques. We currently have *n-i-p-i* superlattices subjected to a strong magnetic field in the perpendicular configuration under study and the results will be reported elsewhere.

ACKNOWLEDGMENTS

The author wishes to express his sincere thanks to Dr. P. Halevi for stimulating discussions and to Professor B. Djafari-Rouhani for a useful communication.

APPENDIX

The transfer matrix $\underline{T}$ introduced in Eq. (14) has an explicit form given by

$$\underline{T}=\begin{bmatrix} T_{11} & T_{12} \\ T_{21} & T_{22} \end{bmatrix} , \tag{A1}$$

where

$$\begin{aligned}
T_{11}=&\frac{1}{N}[(P_1e^{D}+P_1'e^{-D})(P_2e^{B}+P_2'e^{-B})e^{C} \\
&+(Q_1e^{D}+Q_1'e^{-D})(R_2e^{B}+R_2'e^{-B})e^{-C}]e^{A} , \\
T_{12}=&\frac{1}{N}[(P_1e^{D}+P_1'e^{-D})(Q_2e^{B}+Q_2'e^{-B})e^{C} \\
&+(Q_1e^{D}+Q_1'e^{-D})(S_2e^{B}+S_2'e^{-B})e^{-C}]e^{-A} , \\
T_{21}=&\frac{1}{N}[(R_1e^{D}+R_1'e^{-D})(P_2e^{B}+P_2'e^{-B})e^{C} \\
&+(S_1e^{D}+S_1'e^{-D})(R_2e^{B}+R_2'e^{-B})e^{-C}]e^{A} , \\
T_{22}=&\frac{1}{N}[(R_1e^{D}+R_1'e^{-D})(Q_2e^{B}+Q_2'e^{-B})e^{C} \\
&+(S_1e^{D}+S_1'e^{-D})(S_2e^{B}+S_2'e^{-B})e^{-C}]e^{-A} ,
\end{aligned} \tag{A2}$$

where

$$N=16n_An_Bn_Cn_D\ , \tag{A3}$$

and

$$\begin{aligned}
&P_1=(n_A+n_D)(n_D+n_C),\quad P_1'=(n_A-n_D)(n_D-n_C)\ ;\\
&Q_1=(n_A+n_D)(n_D-n_C),\quad Q_1'=(n_A-n_D)(n_D+n_C)\ ;\\
&R_1=(n_A-n_D)(n_D+n_C),\quad R_1'=(n_A+n_D)(n_D-n_C)\ ;\\
&S_1=(n_A-n_D)(n_D-n_C),\quad S_1'=(n_A+n_D)(n_D+n_C)\ ;
\end{aligned} \tag{A4}$$

$$\begin{aligned}
&P_2=(n_C+n_B)(n_B+n_A),\quad P_2'=(n_C-n_B)(n_B-n_A)\ ;\\
&Q_2=(n_C+n_B)(n_B-n_A),\quad Q_2'=(n_C-n_B)(n_B+n_A)\ ;\\
&R_2=(n_C-n_B)(n_B+n_A),\quad R_2'=(n_C+n_B)(n_B-n_A)\ ;\\
&S_2=(n_C-n_B)(n_B-n_A),\quad S_2'=(n_C+n_B)(n_B+n_A)\ .
\end{aligned}$$

Here the exponential terms in Eq. (A2) and $n_j, j\equiv A,B,C,D$ are just as defined in Eq. (12) in the text. It is noteworthy that the transfer matrix $\underline{T}$ satisfies the following identity:

$$\det(\underline{T})=1\ . \tag{A5}$$

[1]L. Esaki, in *Synthetic Modulated Structures,* edited by L. L. Chang and B. C. Geissen (Academic, New York, 1985), p. 1.

[2]T. Ando, A. B. Fowler, and F. Stern, Rev. Mod. Phys. **54**, 437 (1982).

[3]R. E. Camley and D. L. Mills, Phys. Rev. B **29**, 1695 (1984).

[4]B. L. Johnson, J. T. Weiler, and R. E. Camley, Phys. Rev. B **32**, 6544 (1985).

[5]R. Szenics, R. F. Wallis, G. F. Giuliani, and J. J. Quinn, Surf. Sci. **166**, 45 (1986).

[6]M. Babiker, N. C. Constantinou, and M. G. Cottam, J. Phys. C **20**, 4581 (1987).

[7]R. Haupt and L. Wendler, Phys. Status Solidi B **142**, 125 (1987).

[8]M. S. Kushwaha, J. Phys. Chem. Solids **49**, 165 (1988).

[9]R. F. Wallis, R. Szenics, J. J. Quinn, and G. F. Giuliani, Phys. Rev. B **36**, 1218 (1987).

[10]R. F. Wallis and J. J. Quinn, Phys. Rev. B **38**, 4205 (1988).

[11]B. L. Johnson and R. E. Camley, Phys. Rev. B **43**, 6554 (1991).

[12]M. S. Kushwaha, Phys. Rev. B **40**, 1692 (1989).

[13]M. S. Kushwaha, Phys. Rev. B **41**, 5602 (1990).

[14]M. S. Kushwaha, Surf. Sci. (to be published).

[15]G. H. Döhler and K. Ploog, *Synthetic Modulated Structures* (Ref. 1), p. 163.

[16]B. L. Johnson and R. E. Camley, Phys. Rev. B **38**, 3311 (1988).

[17]G. A. Farias, M. M. Auto, and E. L. Albuquerque, Phys. Rev. B **38**, 12 540 (1988).

[18]E. L. Albuquerque, P. Fulco, G. A. Farias, M. M. Auto, and D. R. Tilley, Phys. Rev. B **43**, 2032 (1991).